

# Low energy electron scattering from DNA and RNA bases: shape resonances and radiation damage

Stefano Tonzani

*JILA and Department of Chemistry,*

*University of Colorado, Boulder, Colorado 80309-0440*

Chris H. Greene

*Department of Physics and JILA, University of Colorado, Boulder, Colorado 80309-0440*

(Dated: November 15, 2018)

## Abstract

Calculations are carried out to determine elastic scattering cross sections and resonance energies for low energy electron impact on uracil and on each of the DNA bases (thymine, cytosine, adenine, guanine), for isolated molecules in their equilibrium geometry. Our calculations are compared with available theory and experiment. We also attempt to correlate this information with experimental dissociation patterns through an analysis of the temporary anion structures that are formed by electron capture in shape resonances.

PACS numbers:

## I. INTRODUCTION

Reactions induced by electrons drive nearly all the important chemical processes in radiation chemistry, plasma etching in semiconductors, stability of waste repositories, and are also fundamental in the dynamics of the atmosphere and interstellar clouds, with processes such as dissociative recombination and electron attachment.

In recent years, an increasing importance has been recognized to these processes in biological environments, especially in relation to radiation damage to nucleic acids (DNA and RNA). These processes consist in the interaction of ionizing radiation (like  $\alpha$ ,  $\beta$  and  $\gamma$ -rays) with living tissue, generating possibly mutagenic and carcinogenic byproducts, through a wide variety of ionization, excitation and energy transfer processes, that can interest many molecular species in the complex cell environment.

The important work of Sanche and coworkers<sup>1,2,3</sup> has shown that damage to nucleic acids from ionizing radiation<sup>4</sup> (single and double strand breaks in particular) can be generated through a mechanism involving low energy electron attachment to the nucleic acid and subsequent bond breaking due to energy transfer to a vibrational mode of the temporary anion formed in the electron capture step. These low-energy secondary electrons are generated by electron-impact ionization caused by high energy electrons, originally produced directly by the ionizing radiation. In the electron-impact ionization process, the scattered electron loses part of its kinetic energy, while another electron is ejected, with energy much lower than the first one.

In the past few years many studies have been devoted to understanding the mechanism for the action of the low-energy electrons and their capability to cause strand breaks.<sup>5,6,7,8,9</sup> A first general feature on which there is wide agreement is that the electron capture is mainly

due to the DNA and RNA bases. These molecules have extended aromatic systems, therefore there is a wide range of low-lying unoccupied  $\pi^*$  orbitals where an electron can be captured, giving rise to a shape resonance, a temporary anion, in the range of energies between 0 and 15 eV, where the experiments have found signatures of electron-induced damage to nucleic acids.

The simplest of these bases are thymine, cytosine, uracil (pyrimidines, monocyclic) and adenine and guanine (purines, bicyclic and generally larger than pyrimidines). Their structures are shown in Fig. 1. In this paper we will present theoretical predictions of cross sections for elastic electron scattering from these large molecules. Determination of the location, width, and electronic structure of resonances for a single target molecule is an important step towards understanding and possibly modeling the complex dynamics of DNA, which consists of multiple components. Specifically, besides the bases, there are also the sugar backbone, the phosphates, and also the solvation water,<sup>10</sup> that probably plays a major role in stabilizing the temporary anions.<sup>11,12</sup> No previous theoretical or experimental study of low-energy electron scattering from all DNA bases is available for comparison (although a study at intermediate energy has been carried out recently<sup>4</sup>), but our method has proven its reliability in the study of small molecules<sup>13</sup> and more extended systems like  $C_{60}$ ,  $SF_6$  and  $XeF_6$ .<sup>14</sup>

Much experimental work also has been carried out on dissociative electron attachment from DNA bases,<sup>8,15,16</sup> to understand what fragments are generated. We will discuss the possible connections with measured dissociation branching ratios that we can infer from the examination of the spatial shape and nodal surfaces of the resonant wavefunctions.

## II. THEORY

A detailed description of our method is available in Ref. 13. For this reason we will only review here the main points and the changes we have implemented since that work, notably a new polarization-correlation potential<sup>17</sup> which permits enhanced predictive capabilities.

The interaction between the  $N$  electrons in a molecule and the scattered electron is a many body problem that can be recast,<sup>18</sup> using the so called static exchange approximation, into a one body problem for the continuum electron with a nonlocal potential:<sup>13</sup>

$$\left(-\frac{1}{2}\nabla^2 + V_s - E\right)\phi_0(\vec{r}) = \sum_{i,j} c_i c_j \sum_{k=1}^N \phi_{ki}(\vec{r}) \int d\vec{r}' \frac{\phi_{kj}^*(\vec{r}')\phi_0(\vec{r}')}{|\vec{r} - \vec{r}'|} \quad (1)$$

here  $V_s$  is the electrostatic potential,  $\phi_0$  is the scattered electron orbital, while the other orbitals refer to target electrons, and the  $c_i$  are configuration interaction (CI) coefficients. In this approximation only one state for the target is considered (the ground state), whereby it is only suitable to describe electronically-elastic processes. The nonlocal interaction consists of three main pieces: the direct electrostatic contribution, the exchange term and the polarization-correlation potential. Of these three, only the first is a local potential.

To describe electron scattering from a general, possibly very complicated molecule, we use the R-matrix method,<sup>19</sup> which partitions space into two regions: an internal region within which all the short-range physics is confined and an outer region where only long-range interactions (like Coulomb or dipole potentials) are important. Our calculation begins from a variational principle<sup>19</sup> for the logarithmic derivative of the wave function at the boundary between the two regions

$$b \equiv -\frac{\partial \log(r\Psi)}{\partial r} = 2 \frac{\int_V \Psi^*(E - \hat{H} - \hat{L})\Psi dV}{\int_V \Psi^* \delta(r - r_0)\Psi dV} \quad (2)$$

where  $\hat{L}$  is the Bloch operator,<sup>13</sup> and  $r_o$  is the boundary between the internal and external regions. It is possible, after expanding the internal region wavefunction in a suitable basis set, to recast the solution of Eq. 2 as an eigenvalue problem:

$$\underline{\Gamma}\vec{C} = (E - \underline{H} - \underline{L})\vec{C} = \underline{\Lambda}\vec{C}b. \quad (3)$$

The external region is then treated matching the solution of Eq. 3 to the exact wavefunctions for the long-range tail of the molecular potential. We show in Sec. II C how the contribution from a long range dipole field can be included in our method. The basis set we use for the internal region of the  $R$ -matrix is a product of finite element cubic polynomials in all three dimensions, using a grid in spherical coordinates.

### A. Local Density Approximation (LDA)

To simplify further the description of our system we have to deal with the nonlocality inherently present in the potential. To do this we use a local density approximation for the exchange potential, which reduces it to a functional only of the local density:

$$V_{ex}(\vec{r}) = -\frac{2}{\pi}k_F F(k_F, E), \quad (4)$$

where  $k_F$  is the local Fermi momentum:

$$k_F(\vec{r}) = (3\pi^2\rho(\vec{r}))^{1/3} \quad (5)$$

and  $F$  is a functional of the energy and the local density  $\rho(\vec{r})$  (through the local Fermi momentum). The functional form we use for  $F$  is called the Hara exchange.<sup>20</sup> It has been

extensively employed in continuum state calculations, and it is energy-dependent. The local exchange approximation, widely used also in density functional calculations,<sup>21</sup> has proven itself to give qualitatively correct results,<sup>13,18</sup> while being sufficiently simple to implement computationally that it permits an exploration of complex molecular species.

## B. DFT Polarization potential

We have recently added to our computer code the capability to use a parameter free correlation-polarization potential,<sup>22,23</sup> based on density functional theory (DFT) ideas. As shown in Ref. 24 the polarization-correlation contribution is physically related to the distortion-relaxation effect on the molecule generated by the incoming electron. This is extremely important for an accurate description of the scattering process. The long range part of this potential is a simple multipole expansion, of which we retain only the induced dipole polarization terms:

$$V_{pol} = -\frac{1}{2r^4}(\alpha_0 + \alpha_2 P_2(\cos \theta)) \quad (6)$$

where  $\alpha_0$  and  $\alpha_2$  are the totally symmetric and nontotally symmetric components of the polarizability tensor, and are calculated *ab initio* using electronic structure codes.

In the volume where the electronic density of the target is not negligible, this potential is nonlocal. The interaction can be approximated again as a local potential, different forms of which have been suggested in the literature. The one we use is based on DFT (specifically on the LYP potential of Ref. 17) and it has yielded reliable results in the work of Gianturco and coworkers.<sup>25</sup> This form makes use of the electron density, its gradient and laplacian, which have to be calculated for each target molecule. The short and long range potentials are matched unambiguously at the innermost crossing point, whose radius is dependent on

the angles.

### C. Dipole physics

Since the molecules we considered in this work have large electric dipole moments, there is a need to consider the long range effect of the dipole field on the scattered electron. Two possible options might be considered, either extending the boundary of the R-matrix box far out to a region where the dipole potential is very small, which would be extremely time-consuming for our calculations, or matching to outer region functions adapted to the dipole interaction. We choose this second route and, following the example of Clark,<sup>26</sup> we define the matrix of the operator:

$$(l^2 - 2D \cos \theta)\Omega_N = N(N + 1)\Omega_N \quad (7)$$

where  $l$  is the angular momentum operator,  $\theta$  is the angle between the incoming electron and the dipole direction,  $D$  is the dipole moment,  $N(N + 1)$  and  $\Omega_N$  are eigenvalues and eigenfunctions. We expand  $\Omega_N$  in a basis of spherical harmonics to diagonalize the system in Eq. 7. The order of the spherical Bessel functions that are matched in the outer region will be now  $N$  (not an integer, in general) rather than the usual orbital angular momentum quantum number  $l$ . Since the dipole moments of the molecules in question are very large, the dipole plus centrifugal potential becomes attractive for the first few channels which may thus have a complex  $N$ . In such cases we define  $N = -1/2 + i\mu$  and the matching functions will become:<sup>26</sup>

$$\bar{j}_N(kr) = \sqrt{\frac{\pi}{2r}} \frac{1}{\sinh \frac{1}{2}\pi\mu} \text{Im}(J_{i\mu}(kr)) \quad (8)$$

$$\bar{n}_N(kr) = -\sqrt{\frac{\pi}{2r}} \frac{1}{\cosh \frac{1}{2}\pi\mu} \text{Re}(J_{i\mu}(kr)) \quad (9)$$

where  $J_{i\mu}$  is a cylindrical Bessel function. This allows us to keep the functions in Eq. 8 always real, and therefore have real  $K$ -matrices.

It should be mentioned, however, that at extremely low energies these functions oscillate rapidly in energy as  $\sin(\mu \log kr)$ , giving rise to  $K$ -matrices that are not smooth functions of energy. Defining the base pair as in Ref. 27 solves the problem, but since we are not interested in energies below about 0.5 eV in this study, the functions in Eqs. 8-9 will be sufficient.

The dipole plus centrifugal potential is attractive if the value of the dipole moment is larger than a critical value ( $D_c=1.625$  Debye for a nonrotating dipole). In this case the dipole interaction can bind the electron all by itself. In general, when rotation is included, the critical value of the dipole moment to have a bound state is around<sup>28</sup> 2-2.5 D and the number of dipole-bound states is finite. In the case of uracil,<sup>7,11,29</sup> such a dipole-bound state exists at roughly 0.1 eV below the neutral ground state energy, at the equilibrium geometry of the target molecule.

#### D. Calculation details

To calculate the target properties we have used the GAUSSIAN 98 program suite, at the Hartree-Fock (HF) level of theory. We have noticed in the past<sup>13</sup> that CI calculations are in this case much more expensive and make comparatively little difference in the final cross sections. All of the molecules we treat here are spin singlets in their ground state. For the scattering calculations we have used an IBM Power 4 supercomputer, each calculation taking about 6 wall clock hours on 16 processors working in parallel. The size of the matrices



generated is about 180000 by 180000 and the direct solution of the linear system requires about 10 minutes per energy point when distributed over 16 processors. The matrices are very sparse (fewer than 0.5% nonzero elements), and we use a direct sparse factorization method to solve the linear system. The convergence of the calculation is such that incrementing the number of sectors by 30% lowers the energy of the resonances by a further 0.1 eV in uracil; since it is already quite cumbersome to carry out these calculations we deemed this level of convergence as sufficient for the purposes of this study. The geometry of the molecules is chosen to be the equilibrium target geometry, optimized at the HF level with a 6-31G\* basis set.

### III. RESULTS

To our knowledge there are no available experimental data or calculations of low energy electron scattering from the complete set of DNA bases. A study of electron attachment has been presented in Ref. 9 and the resonance positions are clearly marked. Compared to these results, our calculations show resonances shifted typically by about 2 eV higher in energy, but the energy spacing of the resonances is comparable to what is observed in the experiment. Moreover the relative values of the widths of successive resonances resemble the measured widths. There is also a theoretical study at intermediate energies,<sup>4</sup> and calculations for scattering from uracil;<sup>12,30</sup> in the following we compare these results to ours.

We have already mentioned that the heterocyclic DNA bases have many low-lying unoccupied orbitals, so it is not surprising that their elastic cross sections for electron scattering exhibit many shape resonances. These may be viewed as a capture of the scattered electron into one of these antibonding orbitals to form a short lived negative ion state.<sup>31,32</sup>

Since all these molecules have, in their equilibrium configuration, only one symmetry

element - reflection through the molecular plane - we will characterize the resonances as being of  $\sigma$  type (no node in the plane) or  $\pi$  type (when they have instead a node in the plane) rather than using the  $A'$  and  $A''$  labels as is customary for the  $C_s$  group.

### A. Positions and widths of resonances

A general comparison of partial elastic cross sections for all five of these molecules is shown in Fig. 2, while in the following we give a more detailed description and compare with information available in the literature. Also, a plot of total time-delays (see also Sec. IIIB for details) is provided in Fig. 3 to show the resonances in more detail.

Since we are dealing with polar molecules, applying the fixed-nuclei approximation as it stands makes the partial wave expansion of the forward scattering amplitude divergent. Due to the long-range nature of the dipole interaction, in fact, all partial waves would contribute to the scattering process, causing an infinite scattering in the forward direction and therefore infinite integral cross sections. There is a method, extensively discussed in the literature,<sup>33,34</sup> to deal with this problem by means of a Born closure formula, which yields a finite integral cross section once molecular rotations are included. We will not pursue this further, since existing experiments are not likely to deal with such detailed rotational structures. Therefore our cross sections and time-delays include only up to  $l_{max} = 10$  and omit all higher partial waves. The correction would be proportional to the dipole moment and inversely proportional to the smallest rotational spacing. For the DNA bases the dipole moment is large, while the rotational spacing is small. Therefore the correction can be quite large especially at very low energy. The correction would thus tend to mask the resonant structures, which are the most interesting observables and which have been measured in experiments. All of the calculated cross sections grow rapidly when the incident

electron energy decreases below 1 eV, which is a signature of the role played by the dipole field in pulling in the electron and which is very common in electron scattering from polar molecules.<sup>9,35</sup>

A comparison of four resonance patterns with the electron transmission spectroscopy (ETS) data of Burrow and coworkers<sup>7,9</sup> can be found in Figs. 10-12, where the time-delay data from our calculations has been rescaled by an overall constant and shifted down in energy to facilitate the comparison of energies, widths and spacing. All of the resonances obtained in our calculations are listed in Table I.

### 1. *Uracil*

In the cross section of uracil we find 3 resonances, at 2.16 eV (of width 0.2 eV), at 5.16 (0.6 eV wide) and a very broad resonance at 7.8 eV. The resonance at 2.16 eV is dominated by the  $l = 3$  partial wave (50%) and has contributions from  $l = 1$  (35%) and  $l = 2$  (11%). at 5.16 eV the main partial wave is d (66%), at 7.8 eV f-wave is the dominant contribution (64%).

In the work of Gianturco *et al.* (see Ref. 30) three  $\pi^*$  resonances are found at energies of 2.2, 3.5 and 6.5 eV. The second and third  $\pi^*$  resonances from that work fall at lower energies than ours, a somewhat surprising discrepancy since the theoretical models are very similar.

The contribution of the dipole field at distances larger than 12 Bohr is neglected in Ref. 30, but we have noticed that this influences only the overall magnitude of the cross sections (roughly an increase of 20% at very low energy, that is reduced to about 5% around 10eV), the dipole physics only weakly affects the resonance positions and widths.

Resonances are measured Ref. 9 to occur at 0.3, 1.5 and 3.8 eV. They are all assigned as  $\pi$  resonances,<sup>7</sup> so our results should be shifted by about 2 eV down, whereas the spacing

between the resonances is larger than experiment. The relative resonance widths are similar to Ref. 7, in that the first resonance is very narrow, the second broader and the third very broad, a comparison is shown in Fig. 10, where an integration of the experimental data has been performed to show more clearly the resonance positions and widths.

### 2. *Cytosine*

For cytosine we find 3 main resonances, a very sharp one at 1.7 eV (width 0.5 eV), then at 4.3 eV (width 0.7 eV) and a third at 8.1 eV (width 0.8 eV). The dominant angular momentum character of the resonances is the same as for the three corresponding resonances of uracil. Comparing the resonance positions with the data of Ref. 9 we see the same general trend already observed with uracil, of an overall shift higher than experiment of all resonances by about 2 eV. Interestingly, the first two resonances are measured to occur at an energy lower than in uracil, a trend that we verify in our calculations.

### 3. *Thymine*

The scattering cross section for thymine is closely similar to uracil, which is not surprising in view of their close structural similarities, this applies to both the magnitude and the position of the resonances, which are slightly shifted to higher energies. Specifically, we find resonances at 2.4 eV (width 0.2 eV) at 5.5 eV (width 0.6 eV) and at 7.9 eV (width 1 eV).

### 4. *Adenine*

The electron scattering spectrum for adenine presents many resonances, due to the complexity of the target structure, as expected. Also very interesting is the fact that the cross

section drops sharply at energies below 2 eV, a behavior opposite to that found for the other molecules, if we do not consider the dipole physics outside the R-matrix box, whereas a zero-energy peak appears in the full calculation, a possible sign of a dipole bound state right below threshold.

The first resonance occurs at 2.4 eV (width 0.2 eV), the second at 3.2 eV (sharp, width 0.2 eV), then another centered at 4.4 eV (0.3 eV wide), while at 9 eV we have a broader resonance of width 0.5 eV. The dominant partial wave of the first two resonances is  $l = 2$  (65% and 62% respectively). The third resonance is  $l = 3$  at 51% and  $l = 4$  at 33%. The resonance at 9 eV is dominantly  $l = 5$  (53%) with an  $l = 3$  contribution (22%).

Compared to experiment we have a shift of all resonances roughly 1.5 eV higher, as in guanine, in this case the spacings are correct (about 1 eV between the first three resonances, while the fourth falls too high in energy and it is not measured in experiment). Also the experimental widths of the first three resonances are very similar, as in our data. A comparison with the data of Ref. 9 is shown in Fig. 11.

### 5. Guanine

For guanine we find 4 resonances: at 2.4 eV (width 0.2 eV), at 3.8 eV (width 0.25eV), a third at 4.8 eV (width 0.35 eV), then at 8.9 eV (width 0.6 eV) and a broad resonance around 12 eV. Each of the first three resonances has strong contributions from d, f, and g-waves. At 2.4 eV the contributions are 46% for  $l = 2$  and 37% for  $l = 3$ , for the second resonance  $l = 2$  is 44% while  $l = 4$  is 32%, the third is 38% of  $l = 4$  character and 35% of  $l = 3$ . The resonance at 8.9 eV is 33% h-wave, 28% f-wave and 20% g-wave. At 12 eV the composition is:  $l = 4$  and  $l = 5$  equally at 23%, while  $l = 6$  contributes a further 13%.

Comparison to experimental data (see Fig. 12) shows again a shift of 1.5 eV overall,

while the resonance spacing is well reproduced, and the second and third resonances fall at higher energies with respect to adenine, as in our calculations. Also the widths seem close to experiment.

## B. Resonance molecular structures

From the shapes and nodal structures of the resonant states it is possible to attempt a discussion of the dissociation patterns observed experimentally, if we consider the resonant states as being precursors for dissociative states. Caution must be used, though, in drawing conclusions from this analysis, because this involves a certain degree of speculation. In fact, to establish once and for all the dissociation patterns of these complicated systems, scattering calculations at many different geometries would have to be carried out, and the nuclear dynamics should be included, At present this is computationally too expensive to contemplate. The first two resonances observed for uracil are shown in Figs. 4 and 5. The quantity plotted is a projection on the molecular plane of the eigenvector corresponding to the maximum eigenvalue of the time-delay matrix<sup>19</sup>

$$Q = iS \frac{dS^\dagger}{dE}, \quad (10)$$

where  $S$  is the scattering matrix. At the energy where the time delay of the resonance is a maximum, this eigenvector constitutes the dominant contribution to the resonant structure, since it corresponds to the partial wave that experiences the maximum time delay in the scattering process. For sufficiently narrow resonances one eigenvalue is always dominant, making the resonance analysis much easier. The eigenvectors of the time-delay matrix are complex, so we adopt a phase factor such that the highest peak of the wavefunction is a

purely real number. We then find that the resonance wavefunction is real everywhere, to a good approximation (the imaginary part is about  $10^{-6}$  smaller than the value of the real part), and we plot only the real part. We analyze in detail only the cases of uracil and adenine, the other pyrimidines being very similar to the former and guanine to the latter.

The nodal patterns for uracil are very similar to the ones showed in Ref. 30, which is not surprising since the approximations made in that work are similar to ours, as already discussed, therefore we show only the first two resonances. Incidentally, we notice the close resemblance of these resonant wavefunctions to the first virtual orbitals of uracil from a HF calculation performed with a small basis set (6-31G\*), see for example Fig. 6. In Ref. 30 also a very low  $\sigma^*$  resonance is found at 0.012 eV. Our cross section grows substantially at low energy. If we plot the eigenstate corresponding to the largest eigenvalue of the time-delay matrix (as described in Sec. III B), as in Fig. 4, corresponding to this low energy range, it looks similar to Fig. 5 in Ref. 30, with the main differences being that in our wavefunction the N<sub>3</sub>-H bond has a node, there is a large excess charge on N<sub>3</sub> and on the oxygen attached to C<sub>4</sub>, while another nodal surface cuts diagonally from C<sub>2</sub> to C<sub>5</sub>. This resonance anyway does not appear to be so relevant in the experimental data,<sup>7</sup> where mainly the  $\pi^*$  resonances are detected.

We can also see that there is accumulation of electronic density (the peaks of the wavefunction) on the ring structure, and that many of the ring bonds have nodal surfaces cutting through them, so capture in these resonant states can be reasonably thought as leading to a fragmentation of the molecule in which the aromatic ring is broken. Experimental dissociation patterns are illustrated for Br-uracil in Ref. 15, where evidence for breaking of the ring structure lies in the peaks at 1.6 and 3.5 eV produced by (OCN)<sup>-</sup> and other fragments. These fragments can be generated by capture into shape resonances, appearing in our cal-

culations at 2.2, 5.2 and 7.8 eV respectively. In particular there is a nodal surface in the 5.2 eV resonance that encloses the C<sub>4</sub>-N<sub>3</sub> bond, which could generate a CN<sup>-</sup> fragment.

Since our calculations do not take into account core-excited states or vibrations, our results do not include any Feshbach resonant structures. These appear to cause at least some of the patterns observed in experiment, as in the case of uracil,<sup>7</sup> and they will presumably constitute the dominant trapping pathways for energies higher than 7 eV, where the number of electronic Feshbach resonances starts to become very large.<sup>14</sup>

In the case of uracil, we looked carefully for a  $\sigma^*$  resonance that might be similar to the state shown in Fig. 3 of Ref. 7 around 3 eV at equilibrium geometry, a dissociative state most likely responsible for N<sub>1</sub>-H bond cleavage. The Ref. 7 calculation was performed by scaling Hartree-Fock continuum orbital energies, so no information about the width was provided. Such a state, taking into account an expected shift of 2-3 eV upward in our calculations, should have appeared at around 6-7 eV, and it was not found. This is probably due to the fact that this resonance is extremely broad, since it is also not seen even in experiment.<sup>7</sup> Moreover in calculations carried out using complex absorbing potentials, in connection with Green's function methods,<sup>36,37</sup> for similar systems (like benzene<sup>38</sup>), analogous  $\sigma$  resonances were extremely hard to detect. They became narrower (around 1eV width at equilibrium) only when the relevant hydrogen was substituted with a heavy atom like chlorine; this was also demonstrated experimentally in the case of Cl-uracil in Ref. 7.

For adenine there is less experimental information available to compare. In Ref. 16 it is stated that the dominant breakup channel for low energy (0-4eV) electron attachment leads to hydrogen atom loss, and very prominent resonant structures are present in the range 1 to 3 eV. If we look at the resonance wavefunction maps in Fig. 7-9 we can see that there is no significant buildup of electronic density on any of the hydrogens, consistently with the



fact that the negative charge stays on the molecular frame, and therefore there is no  $H^-$  formation.

The first few unoccupied molecular orbitals that can be obtained from a Hartree-Fock calculation for adenine, as in the case of uracil, are extremely similar in their nodal structures to our resonant wavefunctions, so these shape resonances can be viewed quite reasonably as the trapping of the scattered electron in a virtual orbital.

Most of the C-C and C-N bonds have nodal surfaces passing through them, This might suggest that other channels that involve the breakup of C-C and C-N bonds could also be available at these energies, although probably they are less important than the hydrogen loss products.

#### IV. CONCLUSIONS

We have presented results for electron scattering from DNA and RNA bases. In showing some of their resonant wavefunctions, we have attempted to link the molecular breakup patterns and products to the structure of the nodal surfaces of these wavefunctions. The results for cross sections and resonances show an overall shift of about 1.5-2 eV higher for all the resonances in our calculations, compared to experiment, we believe that this shift is due to the approximate nature of our model. Apart from this, though, we seem to reproduce trends observed in experiment, with respect to the resonance spacing, their widths and also in relative positions for different molecules, which gives us guarded confidence in our results. We have presented the first calculations of cross sections for all the main DNA bases, and discussed the relationship of our results to experimental data. Ample room exists for improvement in our model, and it will be desirable to eventually calculate resonant surfaces, and not just equilibrium values, in order to characterize the dissociation processes. Work is

presently underway to meet some of these challenges.

### Acknowledgments

This work was supported in part by the Department of Energy, Office of Science, by an allocation of NERSC supercomputing resources, and by the Keck Foundation through computational resources. We would like to thank P. Burrow, R. Santra and S. Feuerbacher for useful discussions and for sharing their unpublished data.

- 
- <sup>1</sup> B. Boudaiffa, P. Cloutier, D. Hunting, M. A. Huels, and L. Sanche, *Science* **287**, 1658 (2000).
  - <sup>2</sup> P. Levesque, M. Michaud, and L. Sanche, *Nucl. Instr. and Meth. in Phys. Res. B* **225**, 230 (2003).
  - <sup>3</sup> L. Sanche, *Mass. Spectrom. Rev.* **21**, 349 (2002).
  - <sup>4</sup> P. Mozejko and L. Sanche, *Radiat. Environ. Bioophys.* **42**, 201 (2003).
  - <sup>5</sup> R. Barrios, P. Skurski, and J. Simons, *J. Phys. Chem. B* **106**, 7991 (2002).
  - <sup>6</sup> J. Gu, Y. Xie, and H. F. Schaefer III, *J. Am. Chem. Soc.* **127**, 1053 (2005).
  - <sup>7</sup> A. Scheer, K. Aflatooni, G. A. Gallup, and P. D. Burrow, *Phys. Rev. Lett.* **92**, 068102 (2004).
  - <sup>8</sup> F. Martin, P. D. Burrow, Z. Cai, P. Cloutier, D. Hunting, and L. Sanche, *Phys. Rev. Lett.* **92**, 068101 (2004).
  - <sup>9</sup> K. Aflatooni, G. A. Gallup, and P. D. Burrow, *J. Phys. Chem. A* **102**, 6205 (1998).
  - <sup>10</sup> G. M. Blackburn and M. J. Gait, *Nucleic Acids In Chemistry And Biology* (Oxford University Press, Oxford, 1996).
  - <sup>11</sup> T. Sommerfeld, *J. Phys. Chem. A* **108**, 9150 (2004).

- <sup>12</sup> A. Grandi, F. A. Gianturco, and N. Sanna, *Phys. Rev. Lett.* **93**, 048103 (2004).
- <sup>13</sup> S. Tonzani and C. H. Greene, *J. Chem. Phys.* **122**, 014111 (2005).
- <sup>14</sup> S. Tonzani and C. H. Greene, unpublished (2005).
- <sup>15</sup> H. Abdoul-Carime, M. A. Huels, F. Bruning, E. Illenberger, and L. Sanche, *J. Chem. Phys.* **113**, 2517 (2000).
- <sup>16</sup> S. Gohlke, H. Abdoul-Carime, and E. Illenberger, *Chem. Phys. Lett.* **380**, 595 (2003).
- <sup>17</sup> C. Lee, W. Yang, and R. G. Parr, *Phys. Rev. B* **37**, 785 (1988).
- <sup>18</sup> M. Morrison and L. A. Collins, *Phys. Rev. A* **17**, 918 (1978).
- <sup>19</sup> C. H. Greene, M. Aymar, and E. Luc-Koenig, *Rev. Mod. Phys.* **68**, 1015 (1996).
- <sup>20</sup> S. Hara, *J. Phys. Soc. Jpn.* **27**, 1009 (1969).
- <sup>21</sup> R. G. Parr and W. Yang, *Density Functional Theory of Atoms and Molecules* (Oxford University Press, Oxford, 1989).
- <sup>22</sup> F. A. Gianturco and J. A. Rodriguez-Ruiz, *Phys. Rev. A* **47**, 1075 (1993).
- <sup>23</sup> R. Colle and A. Salvetti, *J. Chem. Phys.* **19**, 1404 (1983).
- <sup>24</sup> N. F. Lane, *Rev. Mod. Phys.* **52**, 29 (1980).
- <sup>25</sup> R. R. Lucchese, F. A. Gianturco, and N. Sanna, *Chem. Phys. Lett.* **305**, 413 (1999).
- <sup>26</sup> C. W. Clark, *Phys. Rev. A* **20**, 1875 (1979).
- <sup>27</sup> C. H. Greene, U. Fano, and G. Strinati, *Phys. Rev. A* **19**, 1485 (1979).
- <sup>28</sup> K. D. Jordan and F. Wang, *Ann. Rev. Phys. Chem.* **54**, 367 (2003).
- <sup>29</sup> O. Dolgounitcheva, V. G. Zakrzewski, and J. V. Ortiz, *Chem. Phys. Lett.* **307**, 220 (1999).
- <sup>30</sup> F. A. Gianturco and R. R. Lucchese, *J. Chem. Phys.* **120**, 7446 (2004).
- <sup>31</sup> D. Loomba, S. Wallace, D. Dill, and J. L. Dehmer, *J. Chem. Phys.* **75**, 4546 (1981).
- <sup>32</sup> J. L. Dehmer, *ACS Symposium Series* **263**, 139 (1984).

- <sup>33</sup> F. A. Gianturco, S. Meloni, P. Paoletti, R. R. Lucchese, and N. Sanna, *J. Chem. Phys.* **108**, 4002 (1998).
- <sup>34</sup> C. W. Clark, *Phys. Rev. A* **16**, 1419 (1977).
- <sup>35</sup> J. D. Gorfinkiel, L. A. Morgan, and J. Tennyson, *J. Phys. B* **35**, 543 (2002).
- <sup>36</sup> R. Santra and L. S. Cederbaum, *Phys. Rep.* **368**, 1 (2002).
- <sup>37</sup> S. Feuerbacher, T. Sommerfeld, R. Santra, and L. S. Cederbaum, *J. Chem. Phys.* **118**, 6188 (2003).
- <sup>38</sup> S. Feuerbacher and R. Santra, private communication (2005).

## Figures

FIG. 1: Ground state equilibrium structures of the molecules considered in this paper. The black atoms are oxygens, the dark gray circles represent carbons, the light gray atoms are nitrogens while the small circles are hydrogens.

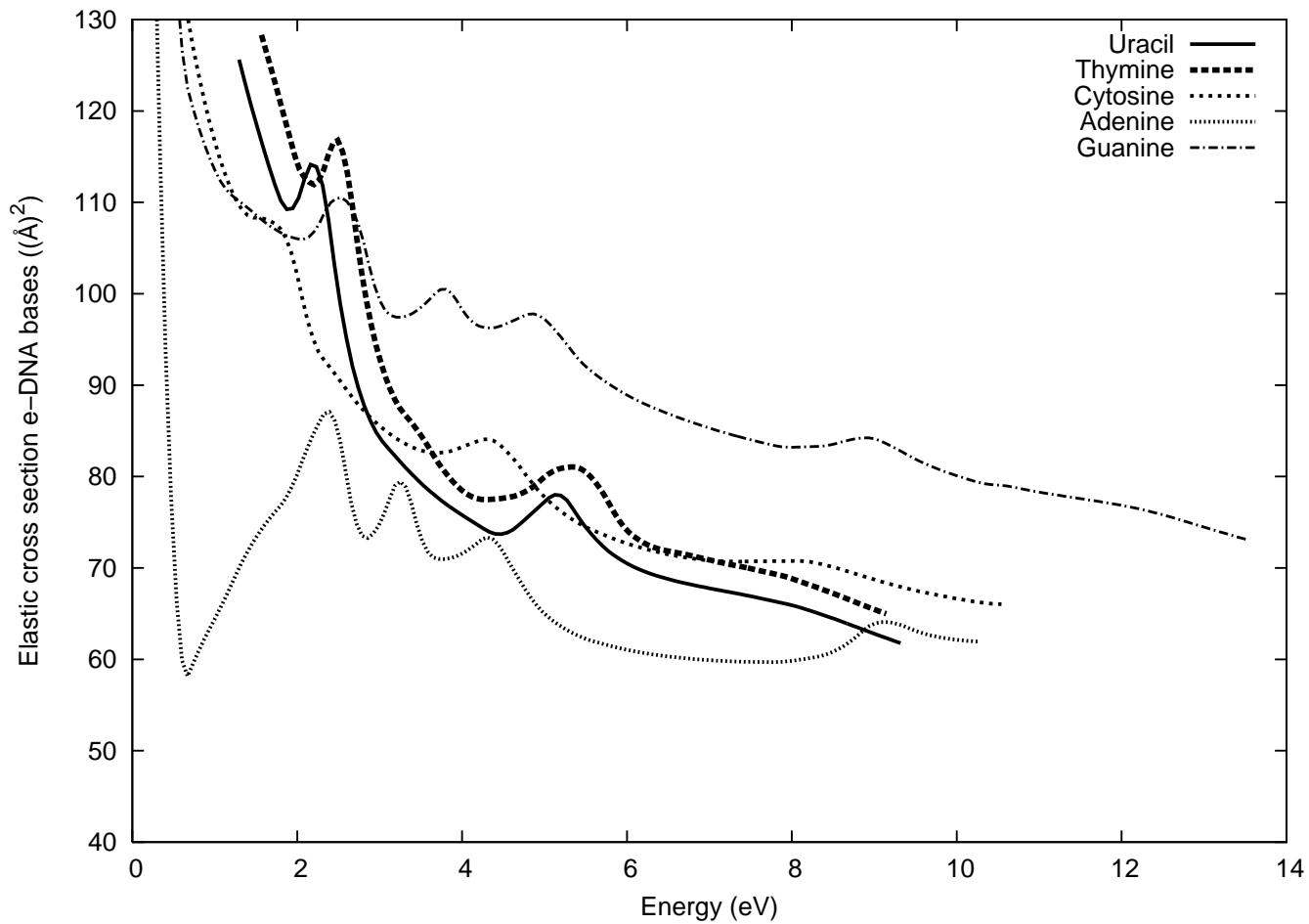


FIG. 2: Partial elastic cross section for the 5 DNA and RNA bases described in the text. Calculations involve partial waves up to  $l = 10$  and the dipole physics outside the R-matrix box is included exactly.

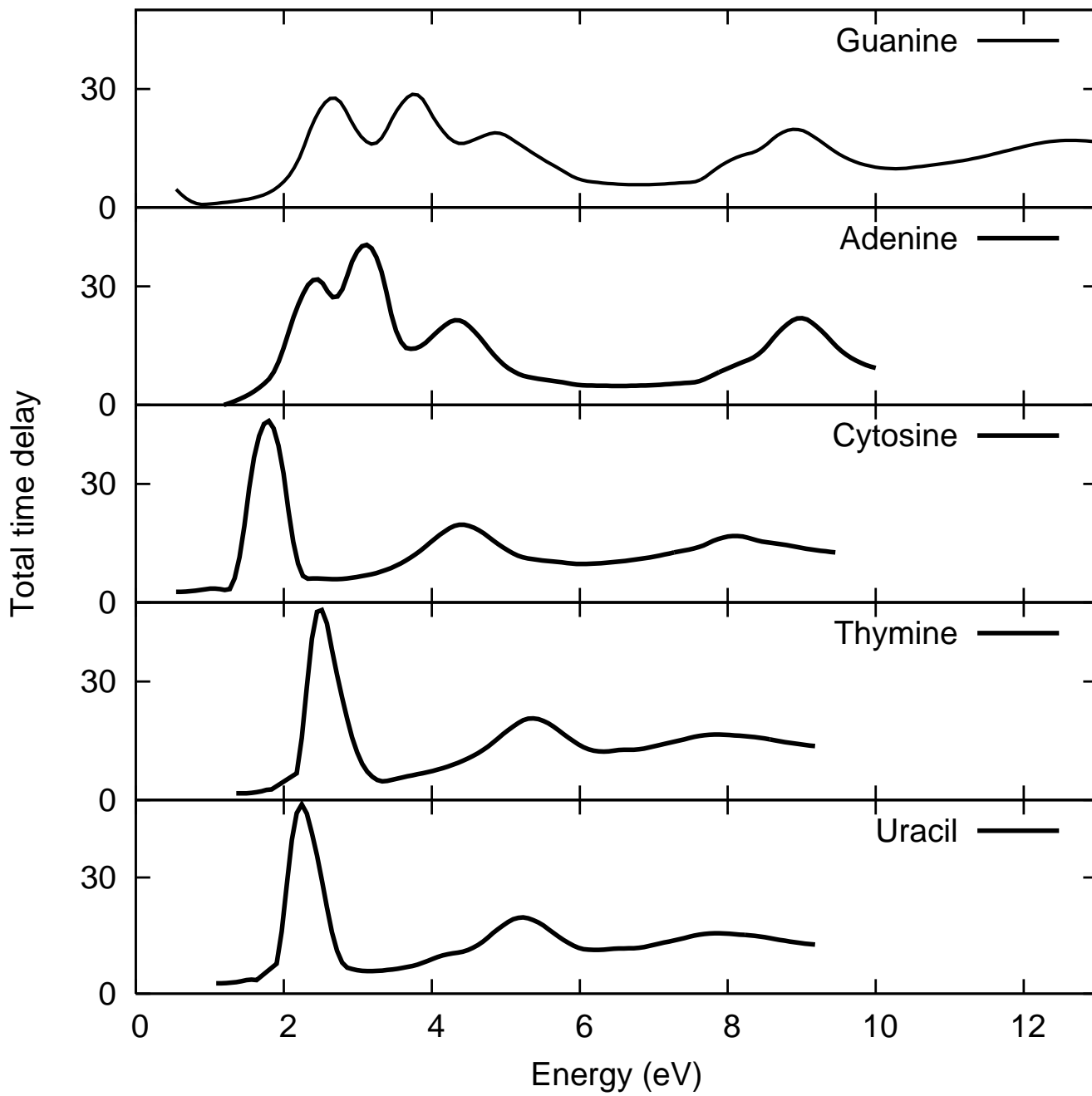




FIG. 3: Total time-delay for the molecules described in the text.

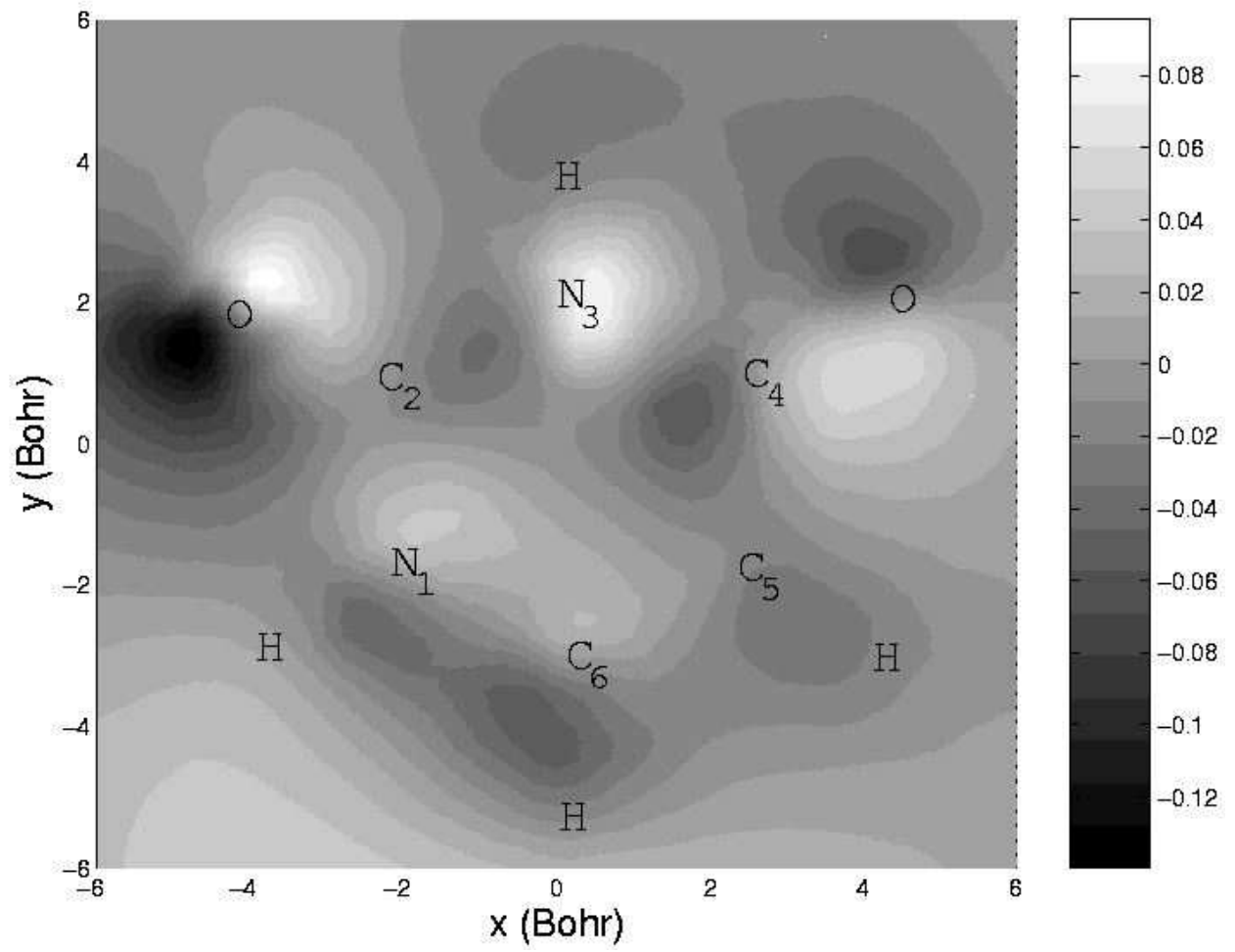


FIG. 4: Uracil: 1st resonance wavefunction. Eigenvector associated to the dominant eigenvalue of the time-delay matrix, as described in the text, for scattering at 0.2 eV.

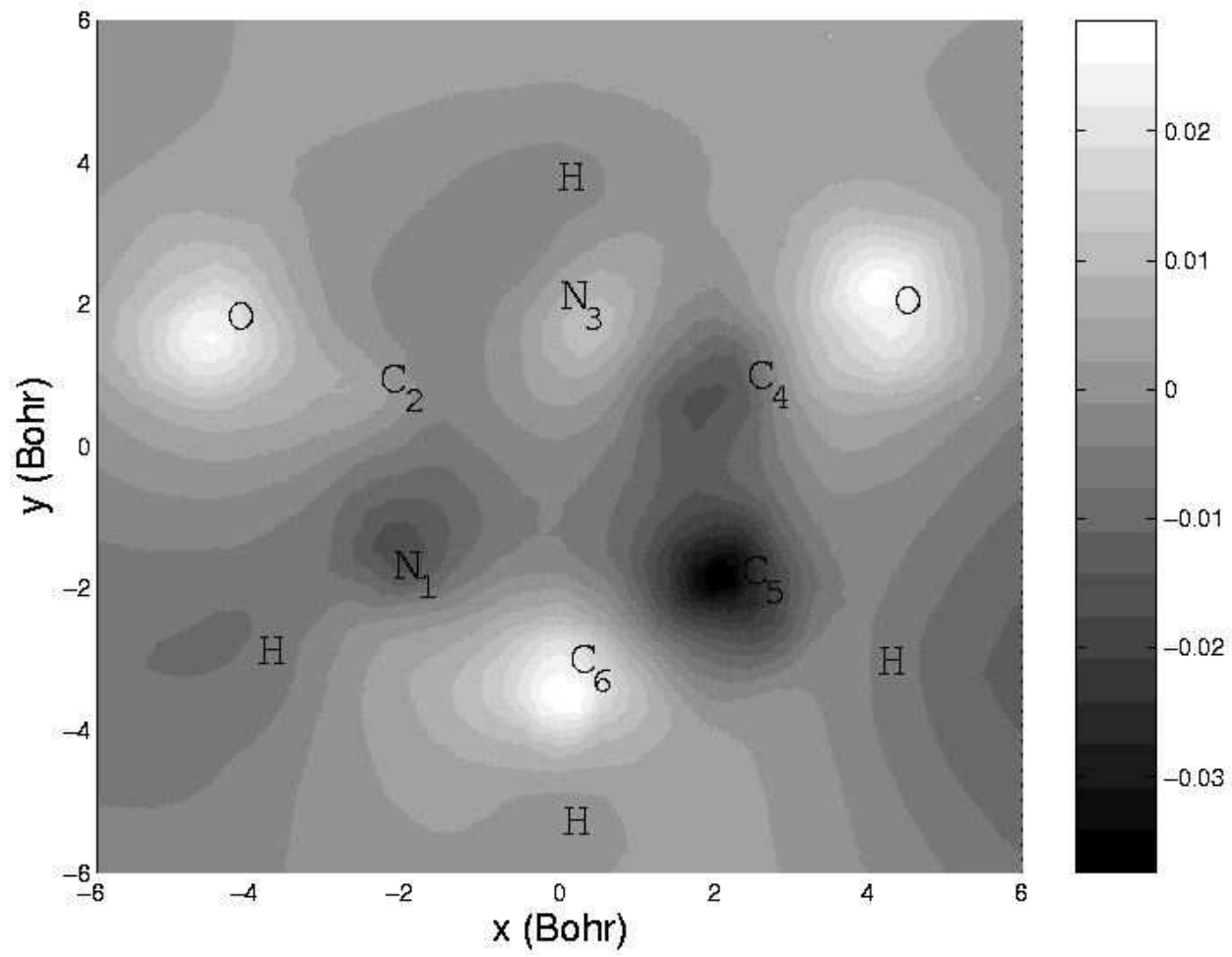


FIG. 5: Uracil: 2nd resonance wavefunction. Eigenvector associated to the dominant eigenvalue of the time-delay matrix, as described in the text, for the resonance at 2.2 eV.

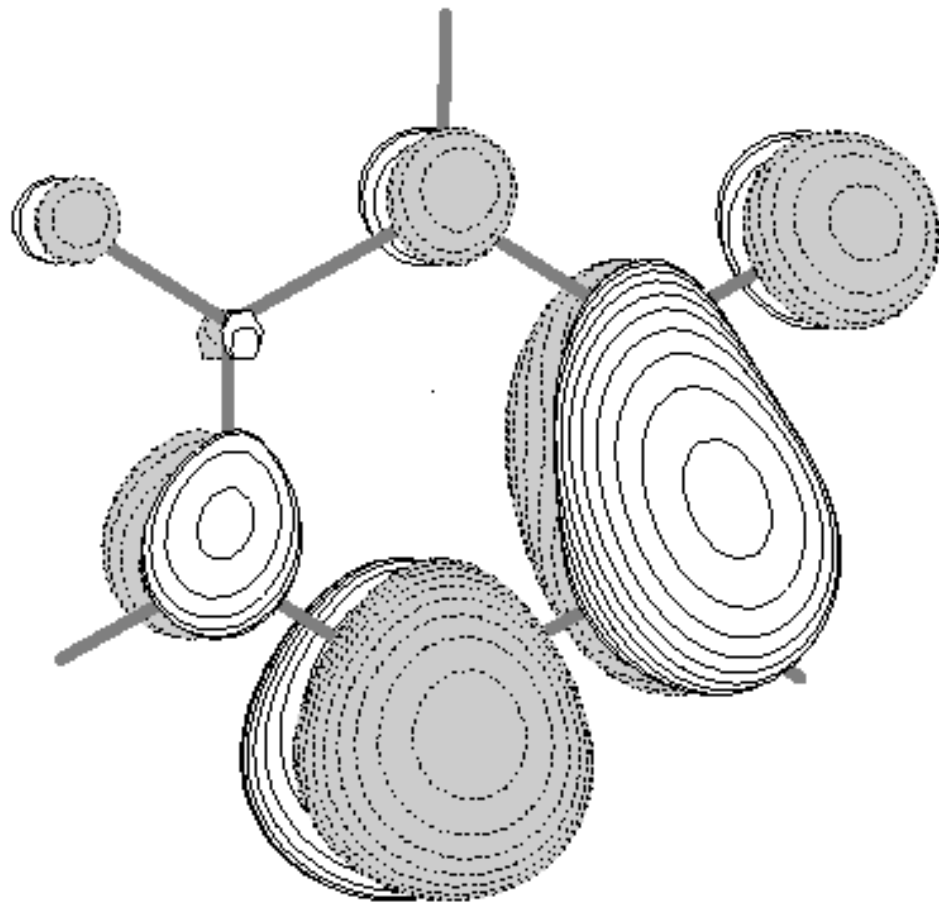


FIG. 6: Uracil: structure of the virtual orbital associated to the resonance at 2.2 eV. The energy of this virtual orbital is 3.42 eV when using a 6-31G\*\* basis set. The orientation of the molecule is the same as in the previous plots. The black and white lobes correspond to opposite signs. It is possible to notice the node in the molecular plane that makes this a  $\pi^*$  orbital.

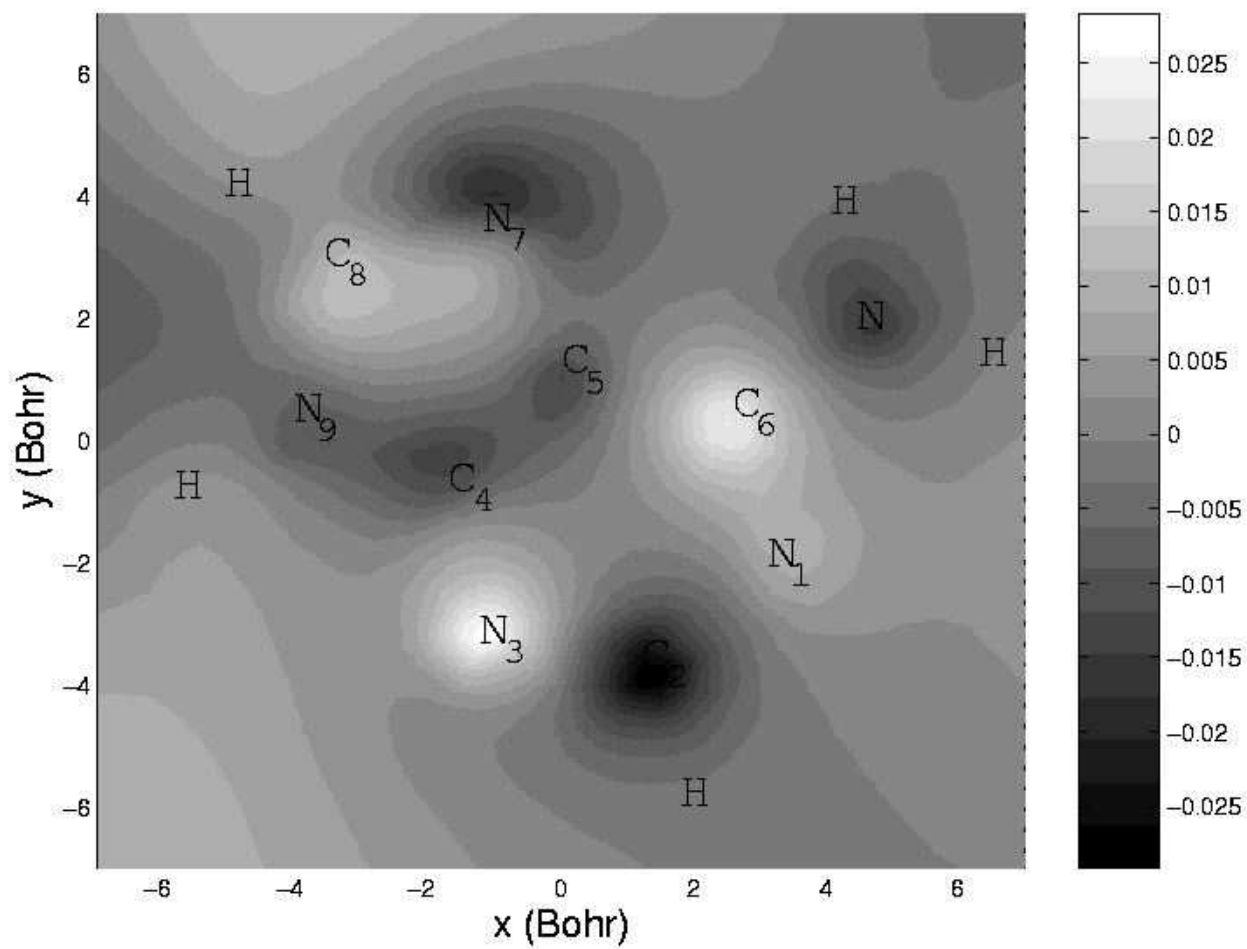




FIG. 7: Adenine: 1st resonance wavefunction. Eigenvector associated to the dominant eigenvalue of the time-delay matrix, as described in the text, at 2.4 eV.

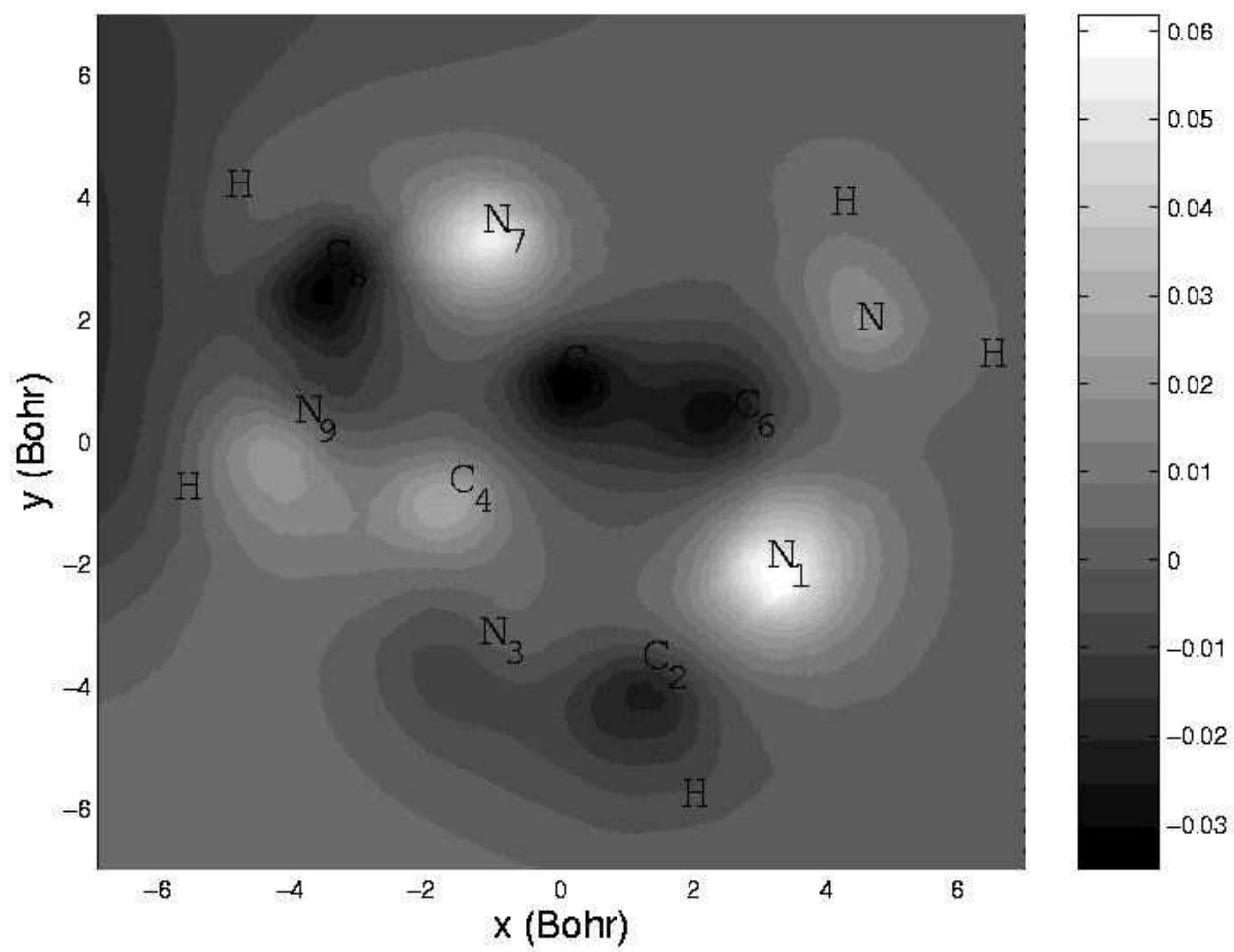


FIG. 8: Adenine: 2nd resonance wavefunction. Eigenvector associated to the dominant eigenvalue of the time-delay matrix, as described in the text, for the resonance at 3.2 eV.

FIG. 9: Adenine: 3rd resonance wavefunction. Eigenvector associated to the dominant eigenvalue of the time-delay matrix, as described in the text, for the resonance at 4.4 eV.

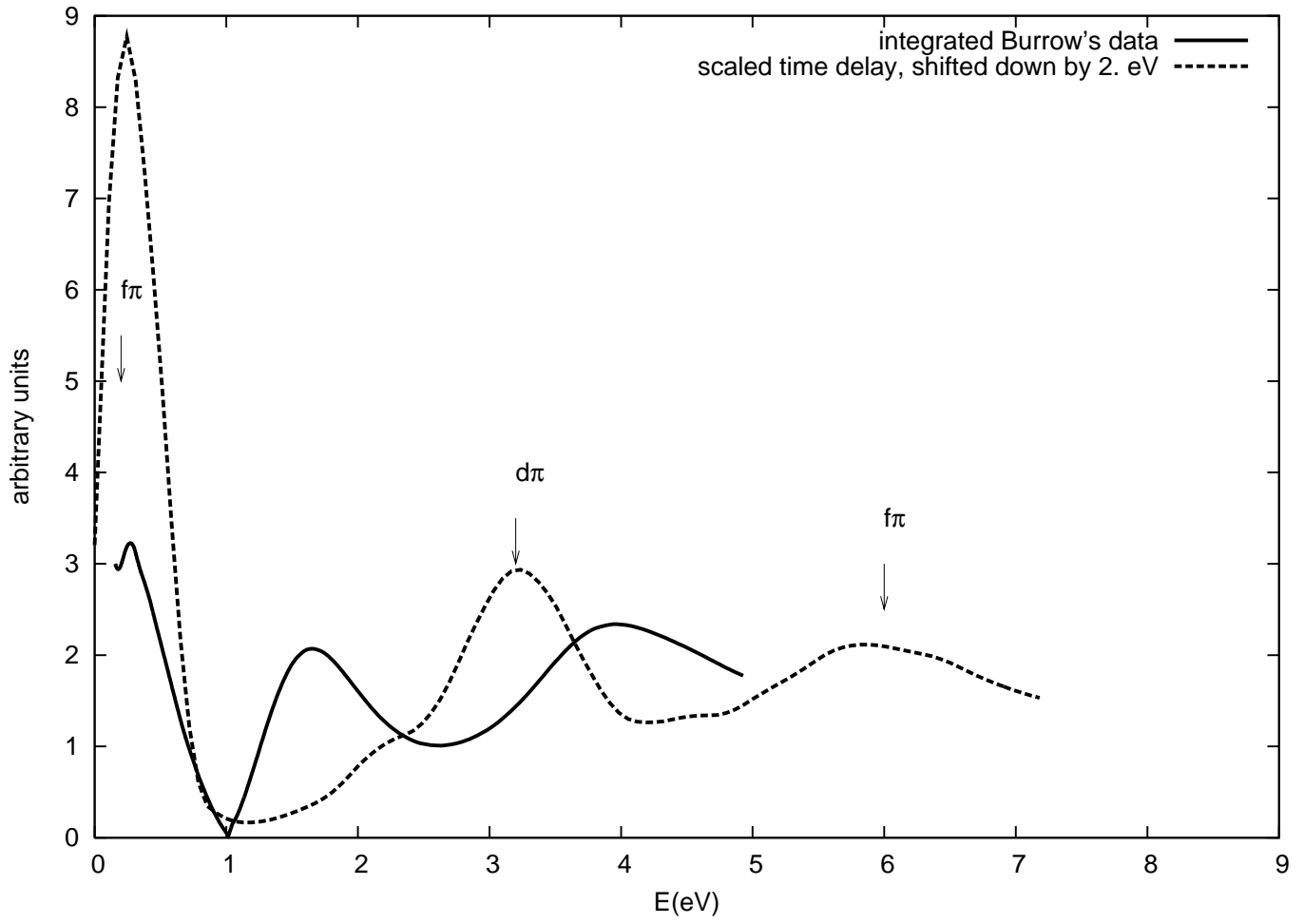


FIG. 10: Comparison with experimental data of Burrow *et al.*<sup>7</sup> for uracil. The arrows indicate resonance positions from the present work, while labels show the dominant partial wave of resonance. The time-delay curve is shifted downward by 2.0 eV to have the position of the first resonance coincide with experimental data.

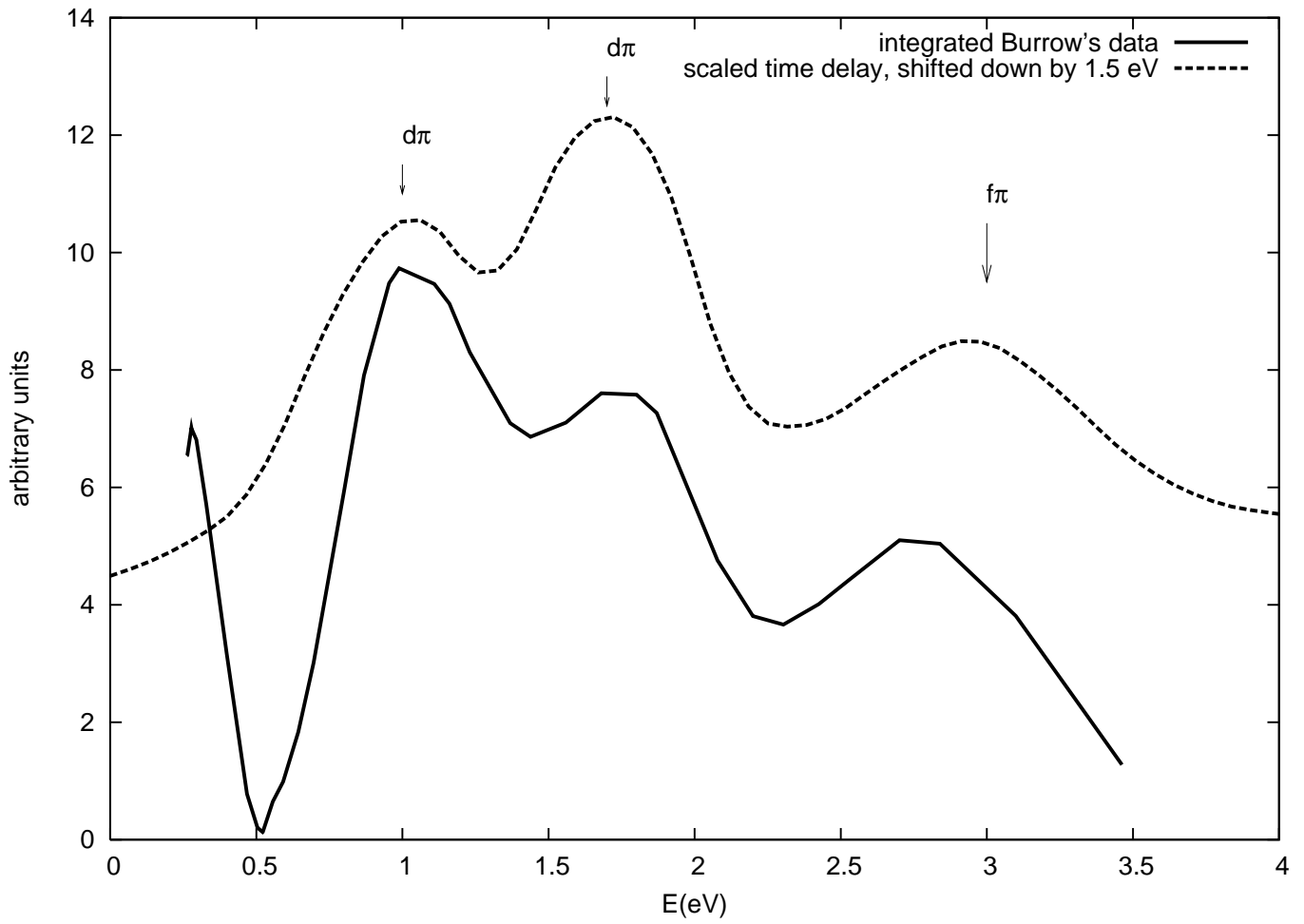


FIG. 11: Comparison with experimental data of Burrow *et al.*<sup>9</sup> for adenine. The arrows indicate resonance positions from the present work, while labels show the dominant partial wave of resonance. The time-delay curve is shifted downward by 1.5 eV to have the position of the first resonance coincide with experimental data.



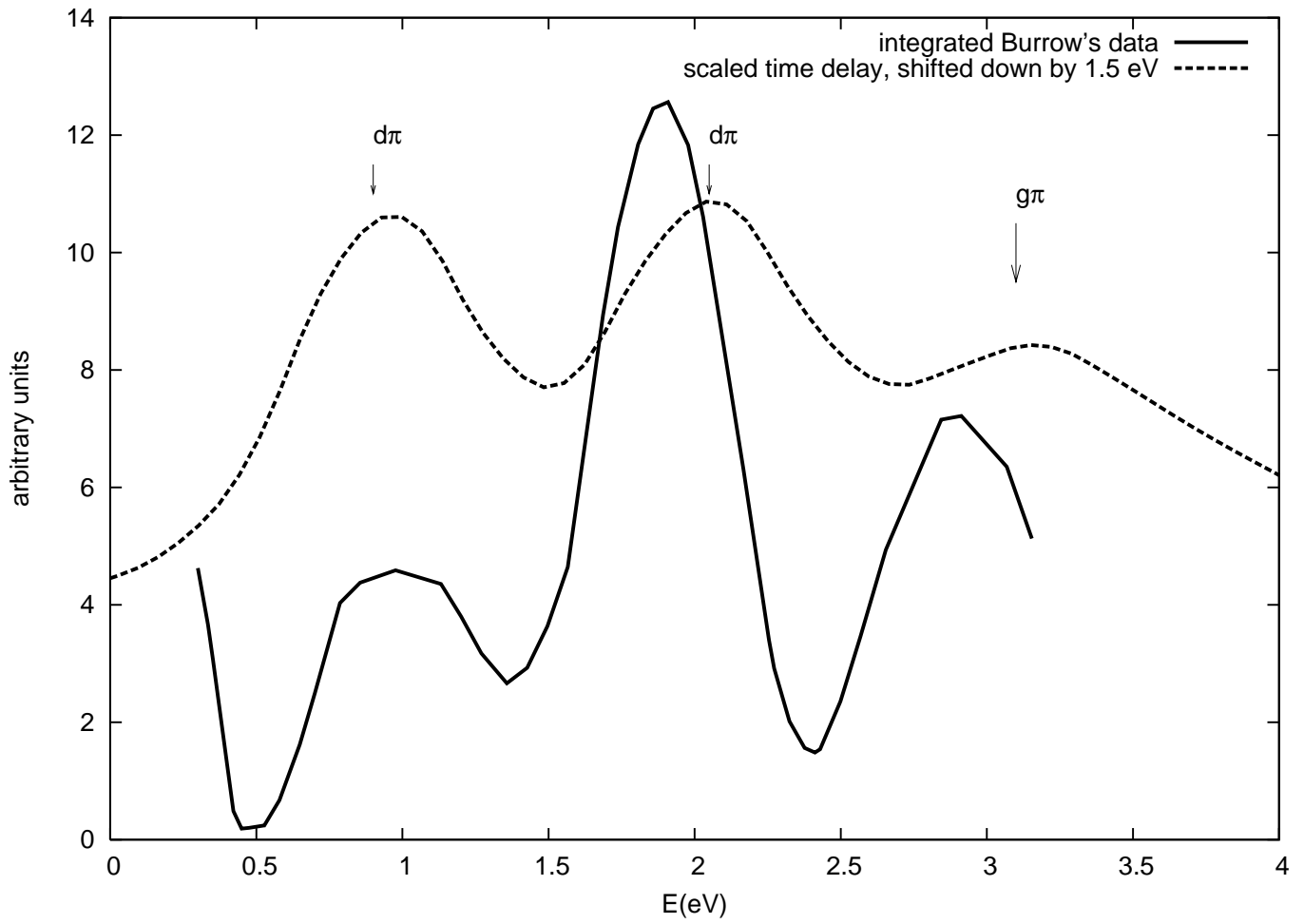


FIG. 12: Comparison with experimental data of Burrow *et al.*<sup>9</sup> for guanine. The arrows indicate resonance positions from the present work, while labels show the dominant partial wave of resonance. The time-delay curve is shifted downward by 1.5 eV to have the position of the first resonance coincide with experimental data.

### Tables

Molecule	Energy (eV)	Width (eV)	Partial wave
<i>Uracil</i>	2.16	0.2	3 (50%)
	5.16	0.6	2 (66%)
	7.8	0.9	3 (64%)
<i>Thymine</i>	2.4	0.2	3 (53%)
	5.5	0.6	2 (62%)
	7.9	1.0	3 (61%)
<i>Cytosine</i>	1.7	0.5	3 (51%)
	4.3	0.7	2 (68%)
	8.1	0.8	3 (63%)
<i>Adenine</i>	2.4	0.2	2 (65%)
	3.2	0.2	2 (62%)
	4.4	0.3	3 (51%)
	9.0	0.5	5 (53%)
<i>Guanine</i>	2.4	0.2	2 (46%)
	3.8	0.25	2 (44%)
	4.8	0.35	4 (38%)
	8.9	0.6	5 (33%)
	12	1.0	4,5 (both 23%)

TABLE I: Energies, widths and dominant partial waves of the resonances discussed in the text.